Probability distribution of irradiance for the onset of strong scintillation

Reginald J. Hill

National Oceanic and Atmospheric Administration/Environmental Research Laboratory/Environmental Technology Laboratory, 325 Broadway, Boulder, Colorado 80303-3328

Rod G. Frehlich

Cooperative Institute for Research in Environmental Sciences, University of Colorado/National Oceanic and Atmospheric Administration, Boulder, Colorado 80303-3328

Received September 12, 1996; revised manuscript received January 6, 1997; accepted January 8, 1997

We calculated the probability distribution function (PDF) from simulations for an initially spherical wave propagated through homogeneous atmospheric turbulence. The onset of strong scintillation was calculated. By onset of strong scintillation, we mean conditions of weak scintillation changing to the condition of strong focusing. In addition, one case in the saturation regime was calculated. The simulations' PDF's are compared with several heuristic models of the PDF and are seen to progress from close to log normal for the cases of weakest scintillation to close to the log normally modulated exponential PDF (LNME PDF) for the cases of strong scintillation. The simulations' PDF's are not in agreement with the K PDF for any of the calculated cases. The best agreement was obtained in comparison with Beckmann's PDF [P. Beckmann, *Probability in Communication Engineering* (Harcourt, Brace, & World, 1967)]. Beckmann's PDF varies from being the log-normal PDF for weak scintillation to being the LNME PDF for strong scintillation and progresses further to the theoretically expected exponential PDF in the limit of saturated scintillation. We recommend that simulation be used to predict the irradiance PDF for plane and diverged waves in homogeneous turbulence in preference to using heuristic models. More complicated propagation cases remain in the domain of heuristic argumentation. © 1997 Optical Society of America [S0740-3232(97)02507-6]

1. INTRODUCTION

Laser radiation propagating through turbulence develops spatial and temporal fluctuations of irradiance known as scintillation. By weak and strong scintillation, we refer to irradiance variances less than unity and greater than unity, respectively. (We follow the nomenclature of Ref. 1.) By saturation of scintillation, we refer to the subset of the strong-scintillation regime for which irradiance variance decreases with increasing turbulence level. By the strong focusing regime, we refer to cases for which irradiance variance is near its maximum. The strong-focusing regime is a subset of the strong-scintillation case and occurs for turbulence levels that are intermediate between those causing weak scintillation and those causing saturation of scintillation. Here, we study the probability distribution of irradiance for a diverged wave (essentially, an initially spherical wave) propagating through homogeneous atmospheric turbulence by means of numerical simulation. This study is focused on the progression from weak scintillation to the strong-focusing regime. We call this case the onset of strong scintillation. One case for saturation of scintillation is given in Appendix A.

Flatté *et al.*[2] showed that numerical simulation can accurately predict the probability distribution function (PDF) of irradiance. Flatté *et al.*[2] used numerical simulation to study the case of a plane wave propagating through homogeneous atmospheric turbulence for all cases from weak scintillation through the strong-focusing regime to saturation of scintillation. They also studied the case of the diverged wave for the regime of saturation of scintillation and obtained excellent agreement with experimental data. Our study helps to complete the case of the diverged wave.

A numerical simulation consists of approximating a three-dimensional random medium as a collection of equally spaced, two-dimensional, random phase screens that are transverse to the direction of wave propagation. The wave is propagated through the screens by means of Fresnel diffraction theory in Fourier transform representation. Flatté *et al.*[2] found that numerical simulations contain all the essential physics for predicting irradiance statistics. We[3] have discussed the following facts: (1) simulation uses all of the same assumptions as derivation of equations for moments of the wave field in the Markov approximation; (2) simulation and field–moment methods have the same range of validity; (3) quantitative agreement of simulations with scintillation experiments validates both simulation and fourth-order field–moment methods; and (4) the assumptions used are not as restrictive as they appear.

Flatté *et al.*[2] compared their simulations with the log-normal PDF, which is well established as valid in the limit of weak scintillation, with the exponential PDF, which is the well-known limit of fully saturated scintillation, as well as with the K PDF defined by Refs. 4 and 5 and the log normally modulated exponential PDF (LNME PDF),[6] both of which are proposed as candidates for

strong scintillation. We denote irradiance normalized by its mean value by I and use angle brackets to denote an ensemble average. Thus $\langle I \rangle = 1$. The K PDF is given by[4,5]

$$P(I) = \frac{2}{\Gamma(y)} y^{(y+1)/2} I^{(y-1)/2} K_{y-1}[2(Iy)^{1/2}], \quad (1a)$$

where

$$y = 2/(\langle I^2 \rangle - 2), \quad (1b)$$

K is the modified Bessel function, and $\Gamma(y)$ is the gamma function. The LNME PDF is given by[6]

$$P(I) = \frac{1}{\sqrt{2\pi}\sigma_z} \int_0^\infty \frac{dz}{z^2} \exp\left[-\frac{I}{z} - \frac{\left(\ln z + \frac{1}{2}\sigma_z^2 \right)^2}{2\sigma_z^2} \right], \quad (2)$$

where σ_z^2 is the variance of the logarithm of the modulation. We compare our simulations' PDF's with the log-normal PDF, the K PDF, and the LNME PDF. For our application to the onset of strong scintillation, the exponential PDF is not applicable. However, a PDF capable of evolving from the log-normal PDF to a PDF applicable to strong scintillation is of interest. Such a PDF is Beckmann's PDF,[7] which is discussed in Section 4. There are many other heuristic PDF models that are reviewed by Flatté *et al.*,[2] Churnside and Clifford,[8] and Patrushev and Rubtsova[9] and therefore need not be discussed further.

An important point is that the PDF of irradiance is determined by only two dimensionless parameters for our case of a diverged wave and homogeneous turbulence. A general discussion of this point is given in Ref. 3, as is a discussion of the additional dimensionless parameters required for initially beamed waves and inhomogeneous turbulence. The two dimensionless parameters can be chosen in many ways. However, irradiance statistics and the irradiance PDF exhibit a particularly orderly variation with changes in the parameters if σ^2_{Rytov} and l_0/R_F are the chosen dimensionless parameters.[3] Here, l_0 is the inner scale of turbulence, R_F is the Fresnel scale, and σ^2_{Rytov} is the irradiance variance, including the inner-scale effect, as calculated for the case of very weak scintillation. These parameters are defined more precisely in Section 2. We present the PDF's for various values of these two dimensionless parameters.

This report has been made brief by placing details in Ref. 10. Such details include mathematical properties of Beckmann's PDF and its statistics, graphs of PDF's for cases not shown here, graphs of the product of the PDF with functions showing the statistical significance of the averages of the given functions, tables comparing statistics obtained from both simulation as well as heuristic PDF's, a table of the parameters of Beckmann's PDF for a wide variety of propagation conditions, further discussion of previous literature, etc. Here we concentrate on the basic principles and illustrate the comparison of the simulation with heuristic PDF's.

2. PROPAGATION PARAMETERIZATION

We define the following parameters: λ is the wavelength of the radiation, $k = 2\pi/\lambda$ is the optical wave number, L is the length of the propagation path, z is the position along the path from $z = 0$ at the transmitter to $z = L$ at the receiver, $R_F = \sqrt{L/k}$ is the Fresnel distance, C_n^2 is the refractive-index structure parameter, and l_0 is the inner scale of turbulence. We use Obukhov's[11] definition of inner scale; this definition is also given in Refs. 12 and 13. Briefly, the inner scale is the spacing at which the asymptotic formula for the inertial-convective range of the refractive-index structure function equals its asymptotic dissipation-range formula.

For isotropic turbulence, the refractive-index spectrum $\Phi_n(\kappa)$ can be written as the product of the inertial-range formula and a dimensionless function $f(\kappa l_0)$, where κ is the spatial wave number, i.e.,

$$\Phi_n(\kappa) = 0.033\, C_n^2 \kappa^{-11/3} f(\kappa l_0). \quad (3)$$

The dimensionless function $f(\kappa l_0)$ describes the spectral bump and dissipation range at high wave numbers, and $f(\kappa l_0)$ depends only on the dimensionless variable κl_0. The limit $\kappa l_0 \to 0$ gives the inertial-range formula for $\Phi_n(\kappa)$ because $f(0) = 1$. A theoretical model for $\Phi_n(\kappa)$, and therefore for $f(\kappa l_0)$, is given by Hill,[14] who showed that the model fits data from precision thermometry in atmospheric turbulence to within the accuracy of the data. The function $f(\kappa l_0)$ from this model is shown in the figures in Refs. 12 and 15–19 and need not be shown here.

Atmospheric scintillation experiments have shown that $f(\kappa l_0)$, as given in Ref. 14, must be used to quantitatively predict weak scintillation.[18–23] These experimental results are reviewed in Ref. 24. Recently, experiment[1] and numerical simulation[16] have shown that this model for $f(\kappa l_0)$ is necessary to quantitatively predict strong scintillation from atmospheric propagation. Flatté *et al.*[16] noted that the agreement of the irradiance variance obtained from numerical simulations with that obtained by experiment, as well as with other theoretical calculations, affords confidence in the use of numerical simulation for quantitative prediction of atmospheric scintillation.

We call the irradiance variance in the weak-scintillation limit the Rytov variance and denote it by σ^2_{Rytov}. Formulas for σ^2_{Rytov} in terms of $\Phi_n(\kappa)$ for a spherical wave propagating through locally isotropic turbulence that is homogeneous along the propagation path are given, for instance, in Ref. 3:

$$\sigma^2_{\text{Rytov}} = \beta_0^2 \tilde{\sigma}^2(l_0/R_F), \quad (4)$$

where

$$\beta_0^2 \equiv 0.496\, k^{7/6} L^{11/6} C_n^2, \quad (5)$$

$$\tilde{\sigma}^2(l_0/R_F) \equiv 10.5 \int_0^1 du \int_0^\infty dx\, x^{-8/3} f(x l_0/R_F) \times \sin^2[x^2 u(1-u)/2], \quad (6)$$

where $x = \kappa R_F$ is the dimensionless wave number and $u = z/L$ is the dimensionless propagation-path position.

The quantity β_0^2 in Eq. (5) is the weak-scintillation variance for an inertial range extending over all wave numbers (i.e., for $l_0 = 0$). Thus $\tilde{\sigma}^2(0) = 1$. The dimen-

sionless function $\tilde{\sigma}^2(l_0/R_F)$, as defined in Eq. (6), is manifestly a function of only its one dimensionless argument. Thus, $\tilde{\sigma}^2(l_0/R_F)$ gives the effect of the spectral bump and dissipation range of $\Phi_n(\kappa)$; in other words, it gives the inner-scale effect. Based on the form of $f(\kappa l_0)$ discussed above, Fig. 3 of Ref. 15 shows $\tilde{\sigma}^2(l_0/R_F)$ as a function of its sole dimensionless argument; Fig. 4 of Ref. 12 and Fig. 2 of Ref. 19 show $\tilde{\sigma}^2$ as a function of $\sqrt{\lambda L/l_0} = \sqrt{2\pi}(l_0/R_F)^{-1}$.

In the limit of very weak scintillation, we have[13]

$$\sigma^2_{\text{Rytov}} = {\sigma_I}^2 = \sigma^2_{\ln I} = -2\langle \ln I\rangle, \tag{7}$$

where we define irradiance variance,

$${\sigma_I}^2 = \langle (I-1)^2\rangle, \tag{8}$$

mean of log irradiance,

$$\langle \ln I\rangle, \tag{9}$$

and variance of log irradiance,

$$\sigma^2_{\ln I} = [(\ln I - \langle \ln I\rangle)^2]. \tag{10}$$

3. MODULATED PROBABILITY DISTRIBUTION FUNCTIONS

Modulated PDF's are also called doubly stochastic PDF's, which are a subset of the more general multiply stochastic PDF's. A review of multiply stochastic PDF's is given by Teich and Diament.[25] Here, we describe some general properties of modulated PDF's that are not emphasized by Teich and Diament,[25] but are important when considering Beckmann's PDF.

Consider two PDF's, $P_1(x|\bar{x}, \sigma_x, \ldots)$ and $P_2(y|\bar{y}, \sigma_y, \ldots)$, wherein the vertical bar separates the random variables x and y from the parameters of the PDF's; the means are $\bar{x}$ and $\bar{y}$, and the standard deviations are σ_x and σ_y. The ellipsis dots indicate that the PDF's may have other parameters. A third PDF can be defined by

$$P_3(x|\bar{y}, \sigma_x, \sigma_y, \ldots) = \int \mathrm{d}y\, P_1(x|y, \sigma_x, \ldots) \times P_2(y|\bar{y}, \sigma_y, \ldots), \tag{11}$$

where the integration extends over all values of y. Thus the random variable y modulates the mean of the random variable x. This third PDF is a modulated PDF, *i.e.*, a doubly stochastic PDF.

Consider that P_2 has a single maximum. As $\sigma_y \to 0$, P_2 becomes the Dirac delta function $\delta(y-\bar{y})$ such that the integral is evaluated to produce

$$\lim_{\sigma_y \to 0} P_3(x|\bar{y}, \sigma_x, \ldots) = P_1(x|\bar{y}, \sigma_x, \ldots). \tag{12}$$

Thus P_3 becomes P_1 as $\sigma_y \to 0$ because P_2 modulates the mean of P_1 but not the variance of P_1. Likewise, as $\sigma_x \to 0$, P_1 becomes the Dirac delta function $\delta(x-y)$ such that the integral is evaluated to produce $P_3(x|\bar{y}, \sigma_y, \ldots) = P_2(x|\bar{y}, \sigma_y, \ldots)$. Thus, P_3 becomes P_2 as $\sigma_x \to 0$.

One can thereby generate P_3 such that it becomes P_1 in one limit and P_2 in another limit provided that P_1 and P_2 admit the possibility that their variances can vanish (a counter example is the exponential PDF). It is therefore possible to satisfy a condition that P_3 have two given asymptotic formulas, but the general behavior of P_3 depends on the choices of P_1 and P_2.

The average (*i.e.*, expectation value) of any function $g(x)$ is an integral of the product of the PDF with $g(x)$. For instance,

$$E_1(g; y, \sigma_x, \ldots) \equiv \int \mathrm{d}x\, g(x)\, P_1(x|y, \sigma_x, \ldots), \tag{13}$$

where the notation is as follows. The subscript on E_1 follows from that on P_1, thereby denoting which PDF is involved. The argument list of the average E_1 contains the function g because E_1 is a functional of g, and the list contains the parameters of P_1. Of course, $g(x)$ might depend on some parameters, but we do not list them explicitly. From Eq. (11), the average of $g(x)$ over the modulated PDF is

$$E_3(g; \bar{y}, \sigma_x, \sigma_y, \ldots) \equiv \int \mathrm{d}x\, g(x)\, P_3(x|\bar{y}, \sigma_x, \sigma_y, \ldots), \tag{14a}$$

$$= \int \mathrm{d}y \left[\int \mathrm{d}x\, g(x)\, P_1(x|y, \sigma_x, \ldots)\right] P_2(x|\bar{y}, \sigma_y, \ldots), \tag{14b}$$

$$= \int \mathrm{d}y\, E_1(g; y, \sigma_x, \ldots)\, P_2(y|\bar{y}, \sigma_y, \ldots), \tag{14c}$$

$$= E_2[E_1(g; y, \sigma_x, \ldots); \bar{y}, \sigma_y, \ldots], \tag{14d}$$

where Eq. (14b) follows from definition (11), Eqs. (14a), (14c), and (14d) follow from definition (13), and the integrations over x and y were interchanged.

We have found that Eq. (14d) is an efficient method of obtaining formulas for $E_3(g; \ldots.)$ in closed form for those functions $g(x)$ for which $E_1(g; \ldots.)$ can be expressed in closed form and for which $E_2(E_1; \ldots.)$ can also be expressed in closed form. Specific applications of Eq. (14d) are given in Ref. 10.

4. BECKMANN'S PROBABILITY DISTRIBUTION FUNCTION

Beckmann[7] derived a PDF for the amplitude of a wave propagating in a random medium. His PDF is a modulated PDF like Eq. (11) with P_1 taken to be a Rice–Nakagami PDF and P_2 taken to be a log-normal PDF. Fante[26] recommended Beckmann's PDF for application to scintillation. Milyutin and Yaremenko[27] used scintillation data to determine the parameters of Beckmann's PDF and compared it with PDF data, but their parameters are not presented in a useful manner.[9,10] Churnside and Clifford[8] independently invented Beckmann's PDF, which they call the log normally modulated Rician PDF. They give a method for estimating the parameters of Beckmann's PDF; however, that method is not accurate, as discussed in Ref. 10.

The Rice–Nakagami PDF is

$$P_{\text{RN}}(I) = (r+1)z^{-1} \exp\left[-r-(r+1)\frac{I}{z}\right] \times I_0\left\{\left[4r(r+1)\frac{I}{z}\right]^{1/2}\right\}, \tag{15}$$

where I is the irradiance, z is the mean irradiance, and I_0 is the modified Bessel function.[28] Beckmann[7] and Churnside and Clifford[8] obtained the Rice–Nakagami PDF by assuming that a received field is a superposition of coherent and scattered fields. Churnside and Clifford[8] called r the coherence parameter and identified it with the ratio of squared moduli of coherent to scattered fields; Beckmann[7] gave a similar description of a slightly different parameter. Weak and strong scintillation correspond to $r \to \infty$ and $r \to 0$, respectively.[8] The log-normal PDF is

$$P_{\mathrm{LN}}(z) = \frac{1}{\sqrt{2\pi}\sigma_z z} \exp\left[-\left(\ln z + \frac{1}{2}\sigma_z^2\right)^2 / 2\sigma_z^2\right], \quad (16)$$

where σ_z^2 is the variance of $\ln z$ and the mean of z is unity.[13] Beckmann's PDF is given by[7]

$$P_{\mathrm{B}}(I|r, \sigma_z^2) = \int_0^\infty \mathrm{d}z P_{\mathrm{RN}}(I|z, r) P_{\mathrm{LN}}(z|\sigma_z^2). \quad (17)$$

Subscripts RN, LN, and B are used to refer to the Rice–Nakagami, log-normal, and Beckmann's PDF's, respectively. Comparison of Eqs. (11) and (17) shows that Eq. (17) is a modulated PDF.

Beckmann's PDF reduces to the log-normal PDF in the limit of weak scintillation, as would be expected on the basis of Section 3; this property is discussed in more detail in Ref. 10. For very weak scintillation measured from long propagation paths in the atmosphere, the log-normal PDF has been shown to be accurate.[29,30] Churnside and Frehlich[31] compared Beckmann's PDF with data from atmospheric scintillation; their data were obtained during very weak scintillation using a 50-m propagation path. They showed that it gives good agreement with the data for the locally stationary case.

For strong scintillation, Beckmann's PDF reduces to the LNME PDF.[8,10] The LNME PDF was introduced by Churnside and Hill,[6] who gave a clear heuristic argument for applicability of the LNME PDF for the case of strong scintillation and showed that the LNME PDF is in good agreement with atmospheric scintillation data for the case of strong scintillation of a diverged wave on a 1000-m path. The LNME PDF is in good agreement with numerical simulation of a diverged wave for the case of strong scintillation.[2] The LNME PDF is in better agreement with experiment and simulation for the case of strong scintillation of a diverged wave than is the K PDF.[2,6]

In the limit of saturated scintillation, it is well known that the PDF of irradiance becomes the exponential PDF.[32] Churnside and Hill[6] showed that the LNME PDF reduces to the exponential PDF in the limit of saturated scintillations, as it should; therefore Beckmann's PDF does also. Beckmann,[7] as well as Milyutin and Yaremenko,[27] have also shown that Beckmann's PDF reduces to the exponential PDF in the limit of saturated scintillations. This exponential limit follows from the general considerations that P_{B} becomes P_{RN} as $\sigma_z \to 0$, and Eq. (15) shows that P_{RN} becomes the exponential PDF as $r \to 0$. More details of this limit are given in Refs. 8 and 10.

5. PARAMETERS OF BECKMANN'S PROBABILITY DISTRIBUTION FUNCTION

The parameters of Beckmann's PDF as given in Eq. (17) are the coherence parameter r and the variance of the log-normal modulation σ_z^2. These parameters can be chosen from data or theory in many ways. We choose to determine them from several irradiance statistics that are, in turn, obtained from numerical simulation. Here we give the necessary formulas for r and σ_z^2 in terms of irradiance statistics. We use the notation $\langle g(I)\rangle_{\mathrm{B}}$ for the average of $g(I)$ over Beckmann's PDF, in preference to the more complicated and explicit notation in Eq. (13). In Ref. 10, we give closed-form formulas for several $g(I)$. One formula, which is also given in Refs. 8 and 31, is for $\langle I^n\rangle_{\mathrm{B}}$, where n is an integer such that $n \geqslant 0$. Other formulas given in Ref. 10 are for $\langle \ln I\rangle_{\mathrm{B}}$ and $\langle I^b\rangle_{\mathrm{B}}$, where b is a real number such that $b \geqslant -1/2$. Here only the following formulas are needed:

$$\langle I^2\rangle_B = \exp(\sigma_z^2)(r^2 + 4r + 2)/(r + 1)^2, \quad (18)$$

$$\langle I^{-1/2}\rangle_{\mathrm{B}} = \pi^{1/2}(r + 1)^{1/2} \exp(-r/2) \times I_0(r/2)\exp(3\sigma_z^2/8), \quad (19)$$

$$\exp(\langle \ln I\rangle_{\mathrm{B}}) = [r/(r + 1)] \times \exp\left[-\frac{1}{2}\sigma_z^2 + E_1(r)\right], \quad (20)$$

where the exponential integral function is defined by[28]

$$E_1(r) \equiv \int_r^\infty \mathrm{d}t\, t^{-1} \exp(-t). \quad (21)$$

Formulas (18)–(20) are derived in Ref. 10 by use of the general procedure in Eq. (14d). Any two of the formulas [Eqs. (18–20)] can be used to determine the unknowns r and σ_z; details are given in Ref. 10. In particular, ratios of powers of two of the above formulas can eliminate σ_z^2; then a root-finding computer routine determines r from given values of the two statistics. Finally, σ_z^2 is determined from either of the two equations. A solution is not guaranteed. In Ref. 10, we show that solutions are not obtained in some cases of strong scintillation, give reasons why this is so, and show that Beckmann's PDF is essentially the LNME PDF in these cases.

Extensive tables of r and σ_z^2 as functions of l_0/R_F and $\sigma^2_{\mathrm{Rytov}}$ are given in Ref. 10. These tabulated values are amenable to interpolation. Thus, for the case of a point source and homogeneous atmospheric turbulence, Beckmann's PDF can be obtained from turbulence parameters C_n^2 and l_0 and propagation parameters L and k.

6. PROBABILITY DISTRIBUTION FUNCTIONS CALCULATED FROM SIMULATIONS

Our simulations used the spherical-wave algorithm described by Coles *et al.*,[33] who obtained the error scaling by use of simulations with various grid sizes and numbers of phase screens. Our Fresnel distance was 10 grid points. For each realization, we used 20 screens along the propagation path. For the cases $\sigma^2_{\mathrm{Rytov}} \leqslant 2.0$, we used 512

$\times$ 512 grid points per phase screen, and 50 realizations were averaged to produce each PDF. For cases in which $\sigma^2_{\text{Rytov}} = 5.0$, we used 1024×1024 grid points per screen, and 15 realizations were averaged to produce each PDF. Thus, the number of partially correlated irradiance values producing the PDF's was $512 \times 512 \times 50 = 13{,}107{,}200$ and $1024 \times 1024 \times 15 = 15{,}728{,}640$ for the former and latter cases, respectively. The scaling of the numerical errors of the simulations was determined by Coles *et al.*[33] for both the plane-wave and the spherical-wave geometry. The error caused by the finite grid size was determined by the rate of convergence of the simulations to a reference field generated by a very fine grid. For the results presented here, this error is less than 2%. Other numerical effects caused less error in irradiance moments than the error from the finite grid size.

We determine the parameter of the K PDF and of the LNME PDF from the simulations' values of $\langle I^2 \rangle$. Since $\langle I^2 \rangle$ is determined more by large values of irradiance (*i.e.*, values that are significantly greater than the mean irradiance, which is unity), it follows that the K and LNME PDF's will fit the simulations' PDF's better at the larger irradiance values. Had we chosen to fit these PDF's to the simulation by using statistics such as $\langle \ln I \rangle$ and $\langle I^{-1/2} \rangle$, then these PDF's would fit the simulation better at small irradiance because $\langle \ln I \rangle$ and $\langle I^{-1/2} \rangle$ are determined more by small values of irradiance (*i.e.*, values that are significantly less than the mean irradiance, which is unity). To determine the parameters of Beckmann's PDF, we used the simulations' values of $\langle \ln I \rangle$ and $\langle I^2 \rangle$, except for one case for which we used $\langle I^{-1/2} \rangle$ and $\langle I^2 \rangle$; this one case is $\sigma^2_{\text{Rytov}} = 5$ and $l_0/R_F = 0.0$. Thus Beckmann's PDF is fitted by one statistic that is determined by relatively smaller values of irradiance and one that is determined by larger values of irradiance.

We define σ by the square root of the value of $\sigma^2_{\ln I}$ as determined from a simulation. That is,

$$\sigma \equiv \sqrt{\sigma^2_{\ln I}}, \tag{22}$$

provided that a simulation determined $\sigma^2_{\ln I}$. In contrast, the K, LNME, and Beckmann's PDFs have values of $\sigma^2_{\ln I}$ that differ from σ^2 because the parameters of these PDF's were not determined to constrain $\sigma^2_{\ln I}$ to equal that of a simulation. On the other hand, we determine the log-normal PDF such that its value of $\sigma^2_{\ln I}$ equals σ^2. We use σ to scale the ordinates and abscissas of our figures. Following Flatté *et al.*,[2] we graph σ times the PDF of $\ln I$ on a logarithmic ordinate; of course, this is the same as a graph of σI times the PDF of I on a logarithmic ordinate. Thus one can consider that either the PDF of I or of $\ln I$ is shown. The combination of ordinate and abscissa is chosen such that the log-normal PDF is the same parabola on all graphs.

The PDF of $\ln I$ from the simulation data was binned by using 2000 bins equally spaced in $\ln I$ from $\ln I = -15$ to $\ln I = 5$. We call these bins the elemental bins. No events occurred beyond the bin limits of -15 and 5. For presentation of our figures, we reduced the number of bins to be graphed by averaging the PDF over adjacent elemental bins to produce a single final bin (by averaging, we mean that the sum of the probabilities of the elemental bins was divided by the number of elemental bins). For $\sigma^2_{\text{Rytov}} = 0.06$, five adjacent elemental bins were averaged to produce final bins. For $\sigma^2_{\text{Rytov}} \geq 1.0$, 20 adjacent elemental bins were averaged to produce final bins. Furthermore, below a threshold probability level we added yet more adjacent elemental bins to maintain a minimum number of events in each final bin. For $\sigma^2_{\text{Rytov}} = 0.06$, the threshold was 5×10^{-5}, and for the other cases it was 10^{-3}. Thus the final bins may become larger than 5 or 20 (as the case may be) of the elemental bins at a probability level below the threshold. A few events at extreme large and small values of $\ln I$ were discarded by this procedure; details of the probability of these discarded events are given in Ref. 10.

If the simulated data were spatially uncorrelated, then the estimates of the PDF's would be Poisson random variables. Because the simulated intensities are spatially correlated, it is difficult to determine the confidence limits for the estimates of the PDF. To investigate the statistical validity of the PDF's, we generated many different PDF's for the case of a large second moment. The PDF's were unbiased and displayed similar statistical scatter.

Figure 1 shows the line symbol key for the subsequent figures. Figures 2–5 have insets showing the details of the curves near the peak of the PDF's. Also shown at upper left in the figures are the corresponding values of σ^2_{Rytov}, l_0/R_F, ${\beta_0}^2$, σ, and ${\sigma_I}^2$; σ^2_{Rytov} and l_0/R_F are given because they define the case, σ is given because it scales ordinate and abscissa, and ${\beta_0}^2$ and ${\sigma_I}^2$ are given because they are the most common scintillation descriptors. Parameters of lesser importance (r, ${\sigma_z}^2$, $\langle \ln I \rangle$, $\langle I^{-1/2} \rangle$, $\langle I^3 \rangle$, etc.) are tabulated in Ref. 10. Each simulation's PDF is graphed as circles with the ordinate value equal to the probability of the final bins multiplied by σ and with abscissa values equal to $(\ln I + 0.5\ \sigma^2)/\sigma$, wherein $\ln I$ is the center of the final bins. The curves for the heuristic PDF's are, in fact, line segments that connect points having abscissa values equal to those of the centers of the final bins and having ordinate values equal to the heuristic model's probability integrated over the final bins and multiplied by σ. Thus in each figure the simulation's and the heuristic PDF's are graphed as histograms having identical bins. On some of the figures, one can see a PDF end within the plotting area; this is because the end point is at the center of the leftmost or rightmost final bin, and no final bins exist beyond that bin.

Our figures are similar in appearance to those of by Flatté *et al.*[2] However, our choice of ordinate and abscissa differs from that of Flatté *et al.*[2] and therefore requires some explanation. Flatté *et al.*[2] presented the PDF's versus $(\ln I - \langle \ln I \rangle)/\sigma_{\ln I}$, where $\langle \ln I \rangle$ and $\sigma_{\ln I} \equiv \sqrt{\sigma^2_{\ln I}}$ differ for each PDF plotted. Thus their abscissa and ordinate have slightly different meanings for each PDF plotted; a specific example was given in Ref. 10. We graph every PDF scaled by its respective simulation's value of σ, and the abscissa for every PDF is $(\ln I + 0.5\ \sigma^2)/\sigma$, where σ is the value from the respective simulation and $\ln I$ is the value at the center of each final bin. Thus, if two curves coincide in our figures, then the two PDF's are equal at the same value of $\ln I$. In each figure we choose the log-normal PDF to have the same value of $\sigma^2_{\ln I}$ as our simulation. Thus in our figures the

log normal is always the same curve and serves as a reference. In the figures by Flatté *et al.*,[2] the log-normal PDF is the same curve on all figures; the same is true for the exponential PDF. That an exponential PDF is not the same curve on all of our figures is of little concern because we treat the onset of strong scintillation, whereas the exponential PDF applies to the asymptotic case of fully saturated scintillation. The appearance of the exponential PDF on our figures is the same as the dashed–dotted curve in Fig. 3.

Figures 2(a) and 2(b), respectively, show our cases for $l_0/R_F = 0$ and 1.0 for our smallest value of Rytov variance, namely, 0.06. For Figs. 2(a) and 2(b) and all subsequent figures, the intermediate inner-scale case, $l_0/R_F = 0.5$, is given in Ref. 10. Only Beckmann's, the log-normal, and the simulations' PDF's are shown in Figs. 2(a) and 2(b) because the LNME and the K PDF's do not exist for irradiance variance less than unity. One can see that the simulations' PDF's noticeably depart from the weak-scintillation asymptote of a log-normal PDF even for σ^2_{Rytov} as small as 0.06 and that Beckmann's PDF is in better agreement with the corresponding simulation's PDF than is the log-normal PDF. Increasing inner scale from Fig. 2(a) to Fig. 2(b) causes the PDF's to become closer to the log-normal PDF, even though the statistical moments change very little as l_0/R_F changes. In interpreting these slight changes, one must keep in mind that the log-normal PDF is determined by the value of σ, whereas Beckmann's PDF is determined by the values of $\langle \ln I \rangle$ and $\langle I^2 \rangle$.

Figures 3(a) and 3(b) show our two inner-scale cases for $\sigma^2_{\text{Rytov}} = 1.0$. The irradiance variance exceeds unity for these and all subsequent figures so that the K and the LNME PDF's can be shown. The irradiance variance is so close to unity for Figs. 3(a) and 3(b) that the K and the LNME PDF's are nearly equal to the exponential PDF, and the K and the LNME PDF's are indistinguishable on the scale of the figures. Therefore the K PDF is not shown in Figs. 3(a) and 3(b). The simulations' PDF's are clearly in disagreement with the log-normal, the K, and the LNME PDF's in Figs. 3(a) and 3(b) and clearly in good agreement with Beckmann's PDF's. An interesting feature of both the simulations' and Beckmann's PDF's is that on the left of the peak of the curves these PDF's appear to approach a straight line as log irradiance decreases. This feature is most pronounced for $l_0/R_F = 1.0$ in Fig. 3(b). This feature is equivalent to the PDF of I having a nonzero value at $I = 0$. Flatté *et al.*[2] also showed this feature, and they showed that it is drastically modified by even slight aperture averaging.

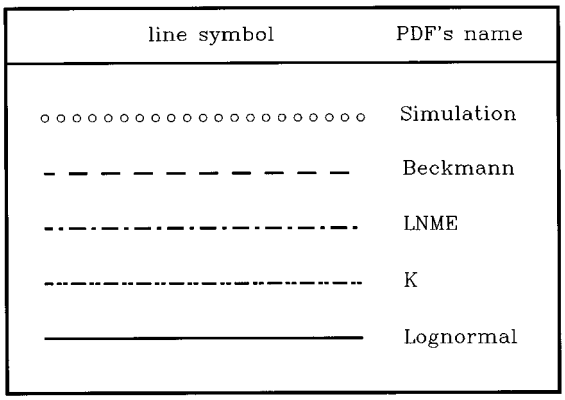

Fig. 1. Curve symbols for figures.

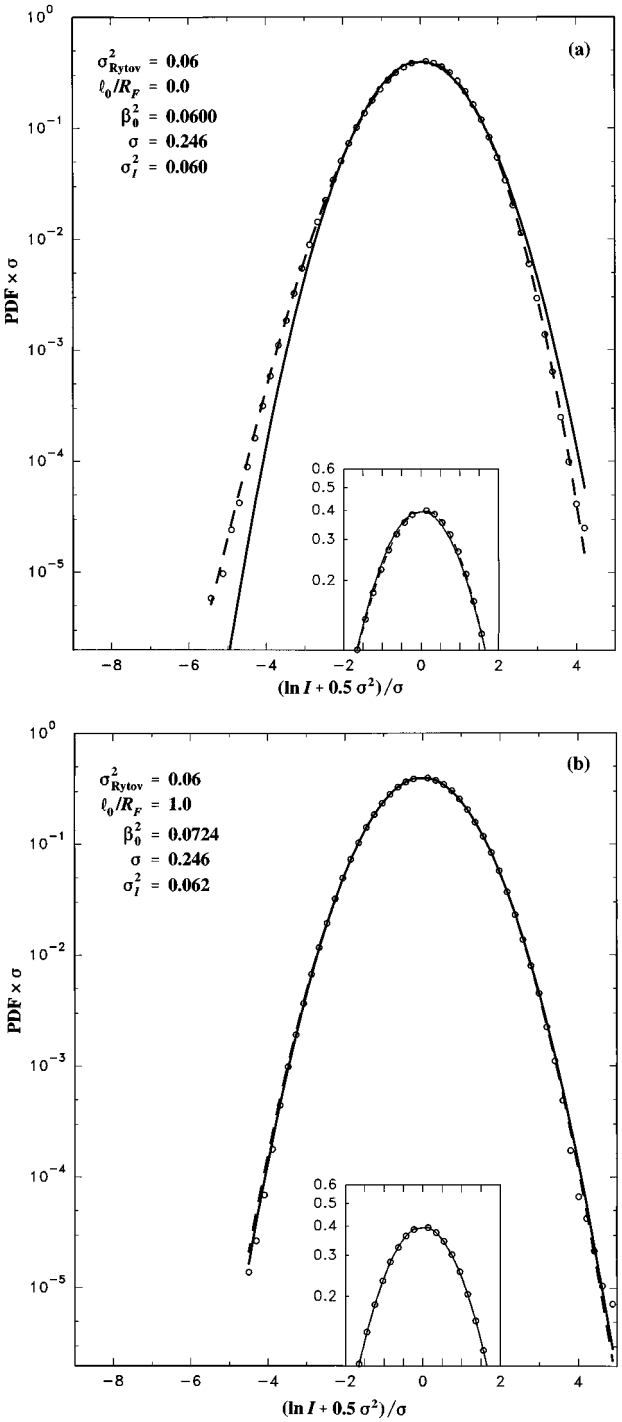

Fig. 2. PDF of $\ln I$ scaled by σ for our case of weakest scintillation. (a) $l_0/R_F = 0.0$ and (b) $l_0/R_F = 1.0$. The simulation, lognormal, and Beckmann's PDFs are shown. Curve symbols are given in Fig. 1. The inset figures give details near the maxima.

Figures 4(a) and 4(b) show our two inner-scale cases for $\sigma^2_{\text{Rytov}} = 2.0$. The LNME PDF is not shown in these figures because it is indistinguishable from Beckmann's PDF on the scale of Fig. 4(a) and would be almost indis-

tinguishable in Fig. 4(b) with the deviations of the LNME PDF from Beckmann's PDF being toward the K PDF. That is, for $\sigma^2_{\mathrm{Rytov}} = 2.0$, Beckmann's PDF has nearly approached its limiting behavior of becoming the LNME PDF. Beckmann's PDF is clearly the closest to the simulations' PDF's in Figs. 4(a) and 4(b), and the LNME PDF is then also close to the simulations' PDF's. The greatest deviation of Beckmann's PDF and the simulations' PDF's is for the case of largest inner scale in Fig. 4(b).

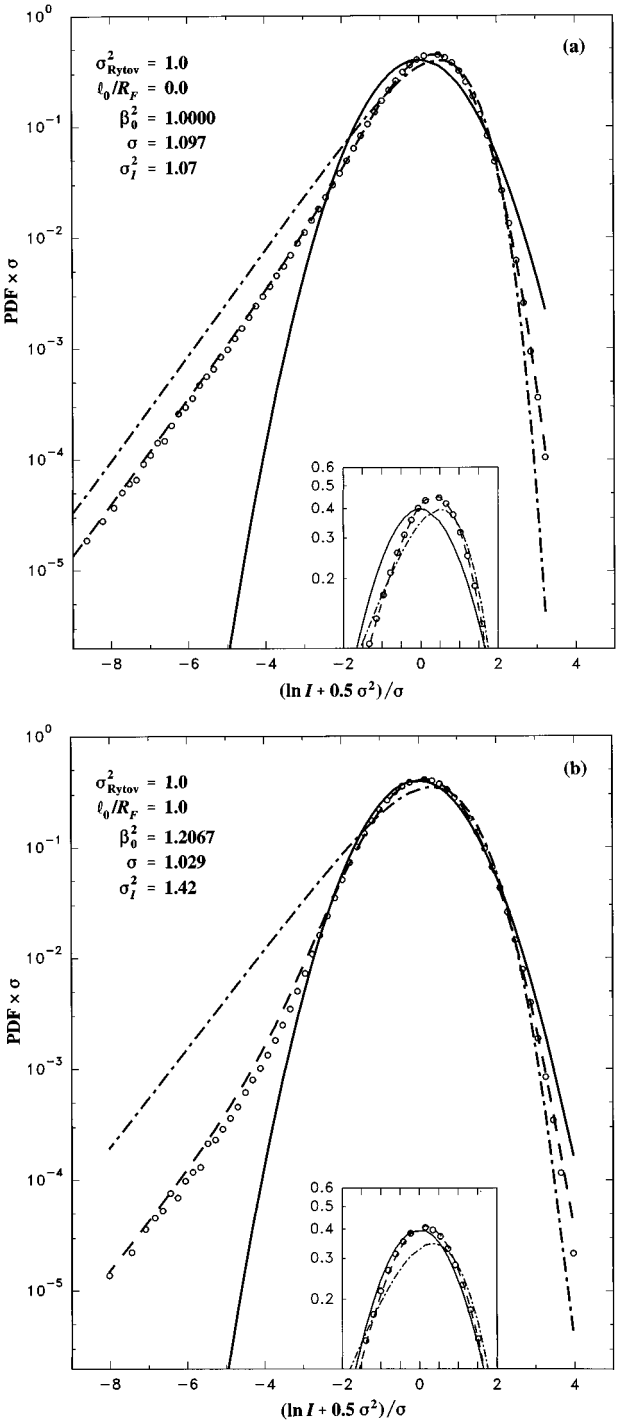

Fig. 3. PDF of $\ln I$ scaled by σ for near-unity variance. (a) $l_0/R_F = 0.0$ and (b) $l_0/R_F = 1.0$. Curve symbols are given in Fig. 1. The K PDF is not shown because it is indistinguishable from the LNME PDF. The inset figures give details near the maxima.

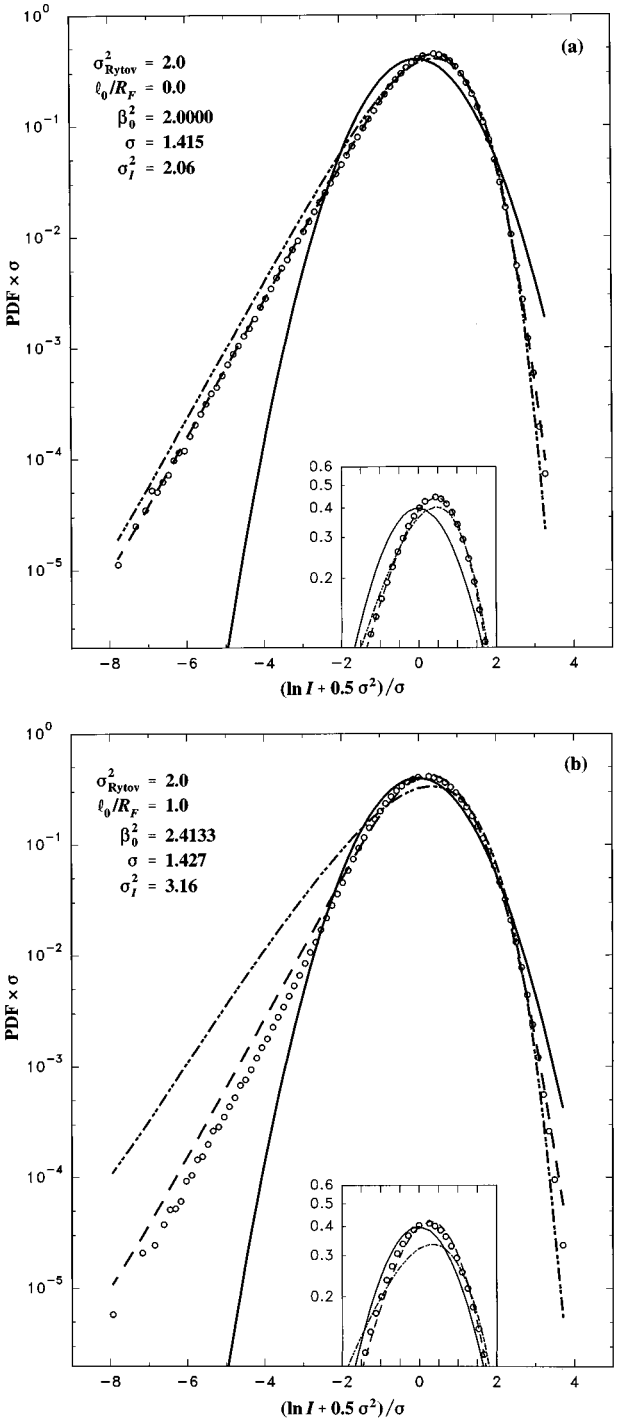

Fig. 4. PDF of $\ln I$ scaled by σ for stronger scintillation than Figs. 2 and 3. (a) $l_0/R_F = 0.0$ and (b) $l_0/R_F = 1.0$. Curve symbols are given in Fig. 1. The LNME PDF is not shown because it is nearly indistinguishable from Beckmann's PDF. The inset figures give details near the maxima.

Figures 5(a) and 5(b) show our two inner-scale cases for $\sigma^2_{\mathrm{Rytov}} = 5.0$. This case is in the strong-focusing regime. The LNME PDF is not shown in Fig. 5(a) because it is indistinguishable from Beckmann's PDF. Beckmann's

PDF is not shown in Fig. 5(b) because fitting its parameters r and ${\sigma_z}^2$ failed for all combinations of statistics that we tried. In fact, for the case in Fig. 5(a), we obtained r and ${\sigma_z}^2$ from $\langle I^{-1/2}\rangle$ and $\langle I^2\rangle$ because we failed to obtain these parameters from $\langle \ln I\rangle$ and $\langle I^2\rangle$ or any other statistics that we tried. Of course, a fit could be forced by some means, such as a least-squares procedure. As scintillation strength increases, the value of r obtained by solving Eqs. (18) and (20) or Eqs. (18) and (19) decreases; as a consequence, Beckmann's PDF approaches the LNME PDF. However, for the case of Fig. 5(b), the deduced value of r is negative; *i.e.*, r has decreased beyond zero, which is the lower bound on r. For negative r, Eq. (17) is not a PDF. That the solution of Eqs. (18) and (20) or of Eqs. (18) and (19) gives a negative value of r is caused by lack of close agreement between Beckmann's PDF and the simulation's PDF. Essentially, Beckmann's PDF must be forced to be the LNME PDF for cases of such large irradiance variance. In Figs. 5(a) and 5(b) we see that the LNME PDF [the same as Beckmann's PDF in Fig. 5(a)] progressively departs from the simulations' PDF's as l_0/R_F increases (and therefore as irradiance variance increases, since σ^2_{Rytov} is fixed[3]), although qualitative agreement remains. The K and the log-normal PDF's are significantly different from the simulations' PDF's in Figs. 5(a) and 5(b). The K PDF fits the simulations' PDF's well on the extreme right-hand sides of Figs. 5(a) and 5(b) and is, in fact, superior to the fit of the LNME PDF in places. Because of the great difference between the K PDF and simulations' PDF's on the left-hand side of Figs. 5(a) and 5(b), we see that if a statistic that emphasizes small values of irradiance is used instead of $\langle I^2\rangle$ to determine the parameter of the K PDF, then the K PDF would disagree substantially on the extreme right-hand sides of Figs. 5(a) and 5(b).

Careful examination of Fig. 5(b) reveals that the circles have error bars. The error bars are plotted only if they exceed the size of the circles and are therefore plotted only at the tails of the simulation's PDF. Each error bar is the standard error of the histogram bin. The 15 statistically independent realizations were binned identically to their average; of course, their average is the simulation's PDF given by the circles. The standard deviation of the 15 realizations was obtained for each bin and divided by $\sqrt{14}$ to obtain the standard error for each bin. The error bars in Fig. 5(b) illustrate the statistical reliability of the simulation's PDF.

The generalized K PDF was introduced by Barakat[34] and further discussed by Jakeman and Tough.[35] This PDF becomes the Rice–Nakagami PDF in one of its limits.[34] Consequently, a log normally modulated generalized K PDF (LNMGK PDF) reduces to Beckmann's PDF in a limit of one of its free parameters. The LNMGK PDF has three free parameters (*i.e.*, one more than Beckmann's PDF) and might be more easily fitted to the simulation in the strong focusing regime, although there is no guarantee that this is so. Consideration of this more complicated heuristic PDF is beyond the scope of the present study. Since two dimensionless parameters determine the PDF,[3] the added complexity of a heuristic PDF having more than two free parameters seems undesirable.

7. CONCLUSION

Numerical simulations require significant expenditure of computational resources. Significant salary is expended for developing heuristic PDF models capable of describing weak through saturated scintillation, as is evidenced by

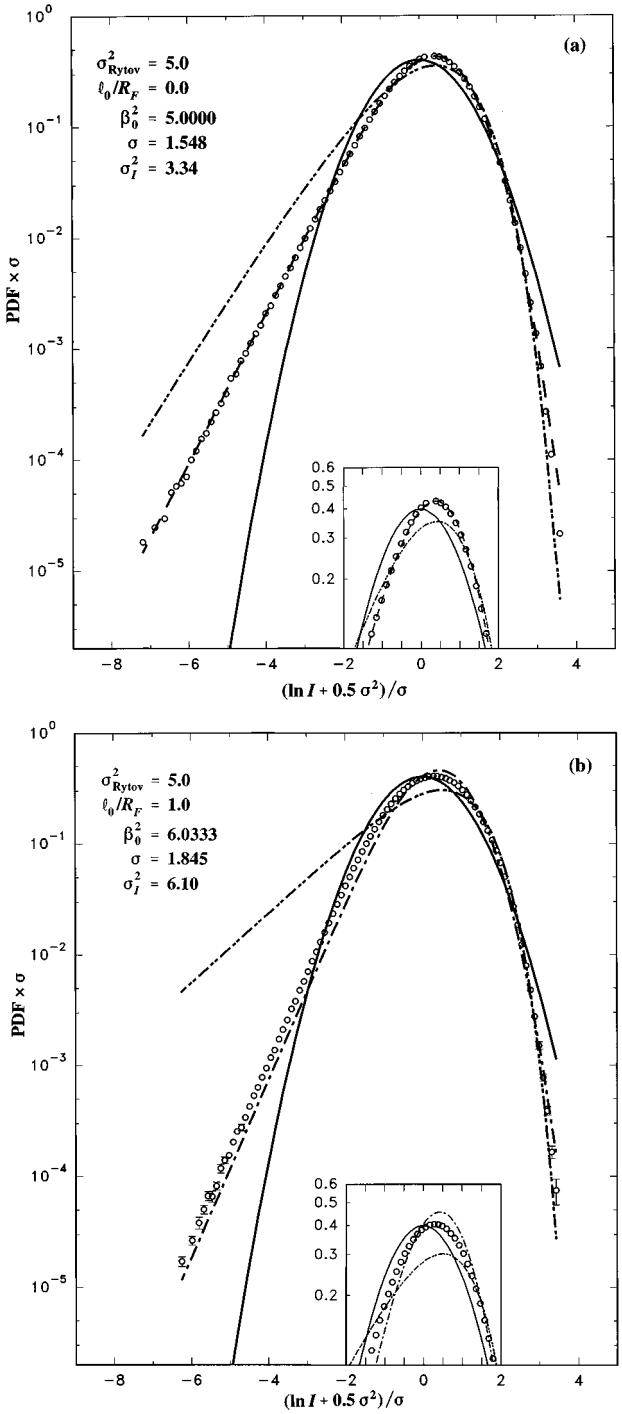

Fig. 5. PDF of $\ln I$ scaled by σ for our case of strongest scintillation in the strong focusing regime. (a) $l_0/R_F = 0.0$ and (b) $l_0/R_F = 1.0$. Curve symbols are given in Fig. 1. The LNME PDF is not shown in (a) because it is indistinguishable from Beckmann's PDF, and Beckmann's PDF is not shown in (b) for reasons given in the text. The inset figures give details near the maxima.

the effort shown in Refs. 8–10, 31, and 33–37. Simulations involve numerical solution of the parabolic-wave equation. Solution of the wave equation is preferable to heuristic argumentation. As shown by the extensive set of irradiance scintillation cases computed by Ref. 3, simulation can produce irradiance PDF's for a wide coverage of the dimensionless parameters $\sigma^2_{\mathrm{Rytov}}$ and l_0/R_F with sufficient density of coverage to allow interpolation, if desired. The case of saturated scintillation for turbulence strengths beyond those calculated by Flatté *et al.*,[2,16] *i.e.*, ${\beta_0}^2 > 60$, become too demanding by present computer standards, so such cases remain the domain of heuristic PDF's. Cases for which more than two parameters are descriptors (such as beamed waves, inhomogeneous turbulence, turbulence intermittency, outer-scale effects, more complicated refractive-index spectra, retroreflector arrays,[9] etc.) are cases that are more demanding of computer resources than our case and remain, for the present, the domain of heuristic argumentation. However, the benchmark cases of initially plane and spherical waves propagating in homogeneous turbulence are amenable to numerical solution of the wave equation by use of the well-established approximations that yield field–moment equations.

Beckmann's PDF is superior to the log-normal and the K PDF's in comparison with the simulations' PDF's. Beckmann's PDF evolves into the LNME PDF for cases of strong scintillation; in fact, we show that Beckmann's PDF has become nearly indistinguishable from the LNME PDF for $\sigma^2_{\mathrm{Rytov}} \geq 2.0$. It has been determined that deriving the parameters of Beckmann's PDF from two statistics fails for strong scintillation, but Beckmann's PDF has already closely approached the LNME PDF for these cases. For such cases, one should take the LNME PDF as the replacement of Beckmann's PDF. Despite the great effort that has been expended on heuristic PDF's, those PDF's do not fit the simulations in detail for all relevant cases. A simulation for the regime of saturation of scintillation is given in Appendix A. In comparison with other results, the results in Appendix A suggest that the K PDF is relatively poor when applied to cases of large irradiance variance, independent of whether the regime of strong focusing or saturation is addressed.

APPENDIX A

We noted the interesting feature in Fig. 3 of the linear appearance of the simulation's PDF at low values of irradiance. By comparing Figs. 3, 4, and 5, we see that this feature becomes more pronounced as irradiance variance is increased. Flatté *et al.*[2] found this feature for plane waves and for the saturation regime of diverged waves. This feature implies that the PDF of I has a nonzero value at $I = 0$. The question arises as to whether our simulation would produce this linear appearance for saturation-regime cases. We present the answer to this question in this appendix.

Flatté *et al.*[2] showed that the K PDF agrees very well with plane-wave simulation PDF's for the case of the saturation regime. In fact, their simulations' PDF's agreed better with the K PDF than with the LNME PDF for their plane-wave cases. On the other hand, for their diverged-wave cases, the LNME PDF agreed substantially better with their simulations' PDF's than does the K PDF. Their saturation-regime, plane-wave cases are for ${\beta_0}^2 = 25$ [where 0.496 in Eq. (5) is replaced by 1.23 for the plane-wave case], and irradiance variances are 1.4–1.8. Their diverged-wave cases are for ${\beta_0}^2 = 23$ and 36, and irradiance variances are 4.35 and 3.17, respectively. For their diverged-wave case, the disagreement with the K PDF is not as extreme as our cases in Fig. 5. Thus, there is more drastic disagreement of the K PDF with the simulations' PDF's for our cases compared with the cases by Flatté *et al.*[2] Is this more drastic disagreement caused by our cases being for the strong-focusing regime as opposed to the saturation-regime cases studied by Flatté *et al.*,[2] or is it because our cases have greater irradiance variance than the cases by Flatté *et al.*[2]?

To resolve these questions, we performed a simulation of a diverged wave for ${\beta_0}^2 = 40$, which is within the regime of saturation of scintillation. We used 4096 $\times$ 4096 grid points per screen and 40 screens on the propagation path; 50 realizations were averaged. The PDF comparisons are shown in Fig. 6. The value of l_0/R_F was 0.8, which produces $\sigma = 1.828$, which is almost the same as the value of σ that pertains to Fig. 5(b), *i.e.*, $\sigma = 1.845$. Thus the ordinates and abscissas of Figs. 5(b) and 6 are quantitatively comparable. For Fig. 5(b), ${\sigma_I}^2 = 6.1$; for Fig. 6, ${\sigma_I}^2 = 5.38$. Since ${\sigma_I}^2$ is chosen to determine the parameters of both the K and the LNME PDF's, it is not surprising that those curves are nearly the same in Fig. 5(b) in comparison with Fig. 6. The simulations' PDF in Fig. 6 is nearly the same as in Fig. 5(b); relative to Fig. 5(b), the circles in Fig. 6 are shifted

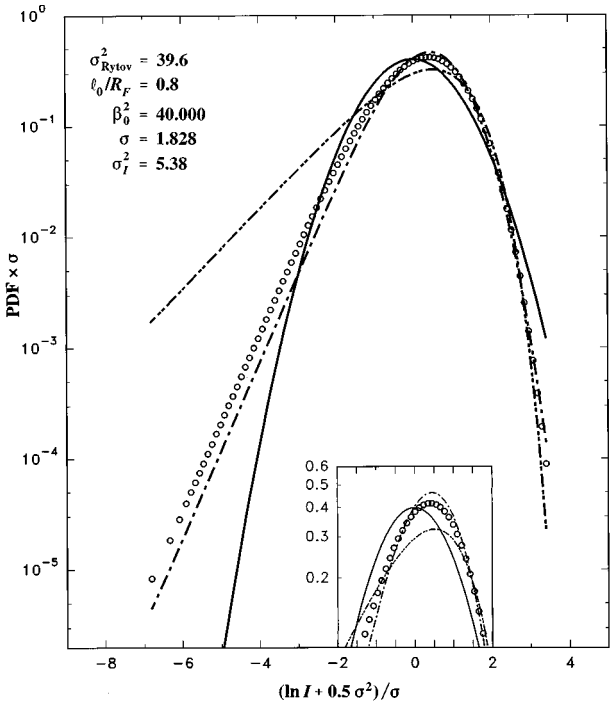

Fig. 6. PDF of $\ln I$ scaled by σ for the regime of saturation of scintillation, with $l_0/R_F = 0.8$. Curve symbols are given in Fig. 1. Beckmann's PDF is not shown for reasons given in the text. The inset figure gives details near the maxima.

slightly to the right near the maximum of the curve and slightly to the left in the left-hand tail of the PDF, with no noticeable change elsewhere. Beckmann's PDF is not shown in Fig. 6 for the same reasons given with respect to Fig. 5(b). For large irradiance variance, our methods do not produce the parameters of Beckmann's PDF.

We find that the linear appearance of the PDF at low values of irradiance on our graphs persists in the regime of saturation of scintillation, as found by Flatté *et al.*[2] We find that the K PDF is a poor representation of the simulation's PDF's because the irradiance variance is large and that it is a poor representation in the saturation regime, as well as in the strong-focusing regime when the irradiance variance is large. Perhaps this is because of some weakness in the heuristic arguments for the K PDF when applied to scintillation. Judging by the results of Flatté *et al.*,[2] the K PDF becomes a worse model than the LNME PDF when the irradiance variance exceeds roughly 2, although the distinction between plane-wave and spherical-wave cases might also be relevant.

ACKNOWLEDGMENTS

This work was partially supported by the National Science Foundation, the U.S. Army Research Office, and the National Aeronautics and Space Administration, Marshall Space Flight Center, under research grant NAG8-253 (Michael Kavaya, Technical Officer).

REFERENCES

1. A. Consortini, F. Cochetti, J. H. Churnside, and R. J. Hill, "Inner-scale effect on irradiance variance measured for weak-to-strong atmospheric scintillation," J. Opt. Soc. Am. A **10**, 2354–2362 (1993).
2. S. M. Flatté, C. Bracher, and G.-Y. Wang, "Probability-density functions of irradiance for waves in atmospheric turbulence calculated by numerical simulation," J. Opt. Soc. Am. A **11**, 2080–2092 (1994).
3. R. J. Hill and R. G. Frehlich, "Onset of strong scintillation with application to remote sensing of turbulence inner scale," Appl. Opt. **35**, 986–997 (1996).
4. E. Jakeman, "On the statistics of *K*-distributed noise," J. Phys. A **13**, 31–48 (1980).
5. E. Jakeman and P. Pusey, "Significance of *K* distributions in scattering experiments," Phys. Rev. Lett. **40**, 546–550 (1978).
6. J. H. Churnside and R. J. Hill, "Probability density of irradiance scintillations for strong path-integrated refractive turbulence," J. Opt. Soc. Am. A **4**, 727–733 (1987).
7. P. Beckmann, *Probability in Communication Engineering* (Harcourt, Brace & World, New York, 1967).
8. J. H. Churnside and S. F. Clifford, "Log-normal Rician probability-density function of optical scintillations in the turbulent atmosphere," J. Opt. Soc. Am. A **4**, 1923–1930 (1987).
9. G. Ya. Patrushev and O. A. Rubtsova, "Probability density of the intensity and flux fluctuations of optical radiation propagating and reflecting in the turbulent atmosphere," Atmos. Oceanic Opt. **6**, 760–769 (1993).
10. R. J. Hill, R. G. Frehlich, and W. D. Otto, "The probability distribution of irradiance scintillation," NOAA Tech. Memo. ERL ETL-274, NOAA Environmental Research Laboratories, Boulder, Colorado (1996). Available from the National Technical Information Service, 5285 Port Royal Road, Springfield, Va. 22161.
11. A. M. Obukhov, "The structure of the temperature field in turbulent flow," Izv. Akad. Nauk. SSSR Ser. Geogr. Geofiz. **13**, 58–69 (1949).
12. R. J. Hill and S. F. Clifford, "Modified spectrum of atmospheric temperature fluctuations and its application to optical propagation," J. Opt. Soc. Am. **68**, 892–899 (1978).
13. V. I. Tatarskii, *The Effects of the Turbulent Atmosphere on Wave Propagation* (Keter, Jerusalem, 1971).
14. R. J. Hill, "Models of the scalar spectrum for turbulent advection," J. Fluid Mech. **88**, 541–562 (;1978).
15. R. J. Hill, "Comparison of scintillation methods for measuring the inner scale of turbulence," Appl. Opt. **27**, 2187–2193 (1988).
16. S. M. Flatté, G. Wang, and J. Martin, "Irradiance variance of optical waves through atmospheric turbulence by numerical simulation and comparison with experiment," J. Opt. Soc. Am. A **10**, 2363–2370 (1993).
17. C. A. Davis and D. L. Walters, "Atmospheric inner-scale effects on normalized irradiance variance," Appl. Opt. **33**, 8406–8411 (1994).
18. E. Azoulay, V. Thiermann, A. Jetter, A. Kohnle and Z. Azar, "Optical measurements of the inner scale of turbulence," J. Phys. D **21**, 541–544 (1988).
19. V. Thiermann and H. Grassl, "The measurement of turbulent surface-layer fluxes by use of bichromatic scintillation," Boundary-Layer Meteorol. **58**, 367–389 (1992).
20. R. J. Hill and G. R. Ochs, "Fine calibration of large-aperture optical scintillometers and an optical estimate of the inner scale of turbulence," Appl. Opt. **17**, 3608–3612 (1978).
21. G. R. Ochs and R. J. Hill, "Optical-scintillation method of measuring turbulence inner scale," Appl. Opt. **24**, 2430–2432 (1985).
22. R. Frehlich, "Laser scintillation measurements of the temperature spectrum in the atmospheric surface layer," J. Atmos. Sci. **49**, 1494–1509 (1992).
23. R. J. Hill and G. R. Ochs, "Inner-scale dependence of scintillation variances measured in weak scintillation," J. Opt. Soc. Am. A **9**, 1406–1411 (1992).
24. R. J. Hill, "Review of optical scintillation methods of measuring the refractive-index spectrum, inner scale, and surface fluxes," Waves Random Media **2**, 179–201 (1992).
25. M. Teich and P. Diament, "Multiply stochastic representations for *K* distributions and their Poisson transforms," J. Opt. Soc. Am. A **6**, 80–91 (1989).
26. R. L. Fante, "Electromagnetic beam propagation in turbulent media," Proc. IEEE **63**, 1669–1692 (1975).
27. E. R. Milyutin and Yu. I. Yaremenko, "Distribution of intensity fluctuation in optical radiation propagating in a turbulent atmosphere," Radiotekh. Elektron. **25**, 2272–2278 (1980). [English translation: Radio Eng. Electron. Phys. **25**, 1–5 (1980).]
28. M. Abramowitz and I. A. Stegun, eds., *Handbook of Mathematical Functions with Formulas, Graphs, and Mathematical Tables* (National Bureau of Standards, Applied Mathematics Series 55, U.S. Government Printing Office, Washington, D.C., 1964).
29. M. E. Gracheva, A. S. Gurvich, S. S. Kashkarov, and V. V. Pokasov, "Similarity relations for strong fluctuations of light in a turbulent medium," Zh. Eksp. Teor. Fiz. **67**, 2035–2046 (1974). [English translation: Sov. Phys. JETP **40**, 1011–1016 (1974).]
30. R. J. Hill, R. A. Bohlander, S. F. Clifford, R. W. McMillan, J. T. Priestley, and W. P. Schoenfeld, "Turbulence-induced millimeter-wave scintillation compared with micrometeorological measurements," IEEE Trans. Geosci. Remote Sens. **26**, 330–342 (1988).
31. J. H. Churnside and R. G. Frehlich, "Experimental evaluation of log-normally modulated Rician and *IK* models of optical scintillation in the atmosphere," J. Opt. Soc. Am. A **6**, 1760–1766 (1989).
32. C. G. Little, "A diffraction theory of the scintillation of stars on optical and radio wavelengths," Mon. Not. R. Astron. Soc. **111**, 289–302 (1951).
33. W. A. Coles, J. P. Filice, R. G. Frehlich, and M. Yadlowsky,

"Simulation of wave propagation in three-dimensional ran dom media," Appl. Opt. **34**, 2089–2101 (1995).
34. R. Barakat, "Weak-scatter generalization of the K-density function with application to laser scattering in atmospheric turbulence," J. Opt. Soc. Am. A **3**, 401–409 (1986).
35. E. Jakeman and R. Tough, "Generalized K distribution: a statistical model for weak scattering," J. Opt. Soc. Am. A **4**, 1764–1772 (1987).
36. L. Andrews and R. Phillips, "I–K distribution as a universal propagation model of laser beams in atmospheric turbulence," J. Opt. Soc. Am. A **2**, 160–163 (1985).
37. L. Andrews and R. Phillips, "Mathematical genesis of the I–K distribution for random optical fields," J. Opt. Soc. Am. A **3**, 1912–1919 (1986).